2
Experimental Techniques

Experimental analysis of molecular interaction has drawn considerable attention in various pure and interdisciplinary research platforms in recent times. As discussed in Chapter 1, amongst several spectroscopic techniques, Nuclear Magnetic Resonance (NMR) has proven to be one of the most efficient spectroscopic methods used to unravel molecular dynamics and interactions both in the solution and in the solid-state. In the present chapter, we provide a brief overview of the theoretical background and experimental setup of various solution-state NMR experiments pertinent for monitoring molecular interaction, association, and aggregation with a particular emphasis on ^{19}F NMR methods employed in this day and age. Solution-state NMR parameters pertaining to chemical shift, relaxation, diffusion, and magnetization transfer are explored in the current Thesis to unveil molecular interactions of small molecules such as ligands and solvents with supramolecular and macromolecular systems. The details of the molecular systems investigated in the Thesis have been provided in Annexure A as table A1, while the specific sample preparation procedures are mentioned in each chapter.

2.1 EXPERIMENTAL SETUP

2.1.1 NMR measurements: All the high field NMR measurements are carried out at 11.7 T (470.5 MHz (^{19}F)/ 500 MHz (^{1}H)) on a Bruker Ascend wide-bore spectrometer equipped with $^{1}H/^{19}F$ double tunable BBFO (Broad Band Fluorine Observation) probehead with z-gradient coils capable of producing z-gradients of up to 51 G/cm. The low field NMR measurements are carried out at *ca*. 0.34 T (corresponding to *ca*. 13.7 MHz (^{19}F) and 14.6 MHz (^{1}H) Larmor frequencies). General description of the NMR methods and pulse sequences used are given in the subsequent sections. In contrast, the specific instrumental parameters used during these NMR experiments for the investigated systems are given in the /respective chapters. The general pulse parameters used during the acquisition of NMR spectra for different nuclei are provided in table A2 of Annexure A. ^{19}F NMR experiments are devoid of solvent suppression, especially water signal that is used as a common solvent for solution preparation. Whereas the suppression of residual solvent signals in ^{1}H NMR is accomplished using off-resonance shaped pulse pre-saturation scheme whenever required.

2.1.2 Other complementary spectroscopic measurements: Various optical spectroscopic methods such as UV-vis spectroscopy and Circular Dichroism (CD) have been employed to obtain complementary and supporting experimental data relevant for the investigated molecular systems. The instrument used and related data analysis are provided in respective chapters.

2.2 NMR PARAMETERS RELEVANT FOR MOLECULAR INTERACTION ANALYSIS

In this section, an introductory description of each of the solution-state NMR methods explored in the current Thesis is presented in terms of a comprehensive theoretical background and experimental design.

2.2.1 Chemical shift and Linewidth

Acquisition of single pulse one dimensional (1D) NMR experiment is well established to detect the number of resonances (signals) arising from chemically and magnetically distinct NMR active species at a particular position (ppm) known as chemical shift. The examination of

chemical shift is the most common aspect of NMR employed for chemical analysis. In solutions, an averaged chemical shift over all molecular orientations are observed due to the faster tumbling (Brownian motions) of molecules on NMR timescale [Derome, 1987; Ludwig and Guenther, 2009; Slichter, 1989]. However, modification in the chemical environment of molecules due to intermolecular interactions manifests a shift in their ppm values either to higher or to lower frequencies. The interaction processes involving a small molecule (ligand) and a macromolecule (target) generally do not induce any change in the covalent structure of the small molecule. Therefore, the perturbations in the chemical shift of ligand on interacting with the target are generally insignificant. On the other hand, the ligand-target interaction can induce measurable perturbation in the chemical shift positions of the target molecule showing gradual shifts in the chemical shift positions during a ligand titration experiment. Such observations have introduced chemical shift perturbation (CSP) as a technique to validate ligand-target interaction unravelling the specific target residues in action [McCoy and Wyss, 2002; Peng, et al., 2004; Williamson, 2013; Yu, et al., 2017]. In the case of the ligand, the possibilities of experiencing hydrogen bonding, short-range contacts, electrostatic interactions and other relevant non-covalent interactions could be distinguished in the free and the target bound state by comparing ligand chemical shift values [Gerig, 1997]. However, such informations are rudimentary for the quantitative analysis of ligand-target interaction.

Unlike the chemical shift values, the tumbling rate of a ligand undergoes significant modification due to interaction with a target, inducing broadening of ligand spectral lines as per the relation $1/\Delta\nu_{1/2} = 1/\pi T_2^*$ [E. D. Becker, 2000; J. Fisher, 2014; Tengel, 2008]. Here, linewidth ($\Delta\nu_{1/2}$) in terms of full width at half maximum (FWHM) is related to apparent transverse relaxation time (T_2^*) that depends on the tumbling of molecule, molecular size, and other physical parameters like viscosity, temperature, and pH of the solution. In case the ligand experiences a slow to intermediate chemical exchange process between its free and target bound states, the existence of at least two different chemical environments becomes inevitable, generating more than one set of chemical shifts for the ligand, and indicating molecular interaction between the ligand-target without ambiguity. Hence, a careful analysis of chemical shift and line broadening can also become effective and may well be used for extracting preliminary quantitative information regarding covalent or non-covalent binding of the ligands to the target [Fielding, 2003]. In general, NMR titration methods based on chemical shift and linewidth are used to decipher the binding events in terms of stoichiometry and binding constant for the ligand-target complex.

It has been well documented in the literature that ^{19}F chemical shift and ^{19}F linewidth are more sensitive towards the local and macroscopic environmental changes compared to that of ^{1}H chemical shift and linewidth due to the presence of a large chemical shift anisotropy (CSA) that also contributes significantly as an active relaxation mechanism in solution in case of ^{19}F [Gerig, 1997]. In the case of small fluorinated molecules, comparatively large differences in ^{19}F linewidth between free and bound state are observed. As stated earlier, it is attributed to the modification of ^{19}F CSA, resulting in very broad lines for bound fluorinated ligands [Fielding, 2007]. Hence, monitoring ^{19}F NMR chemical shift and linewidth is often considered a more sensitive method than ^{1}H NMR to identify binding ligands [Dalvit and Vulpetti, 2011]. Besides such molecular interactions, chemical shift analysis can probe the solution stability of small molecules by simply monitoring the appearance and disappearance of resonances [Dahiya, et al., 2020]. As an example of small molecule-target interaction analysed by probing chemical shift modification and linewidth changes, we chose to characterize the *in vitro* interaction between hexaflumuron (HFM) and β-cyclodextrin (β-CD) [Chaubey and Pal, 2019] in the following.

Cyclodextrins, such as β-cyclodextrin (β-CD) is known to encapsulate small molecules of appropriate sizes in its cavity. The inclusion chemistry is well studied both theoretically and experimentally over several years. These molecular hosts can sequester organic pollutants e.g.,

pesticides, metals etc. from solutions. Both solution and solid-state NMR experiments are potent enough to provide elaborate detailing on the interactions of small molecules with CD and the inclusion mode into the CD cavity [Churchill et al., 2006; Kumar, et al., 2017]. In recent times CDs are used to prepare agrochemical formulations [Villaverde, et al., 2004]. The test molecule HFM chosen as the interaction partner is a multi-halogenated agrochemical. It is a well-known anti-termite pesticide that belongs to benzoylphenlyurea family and consists of three different classes of fluorine, as shown in figure 2.1(a).

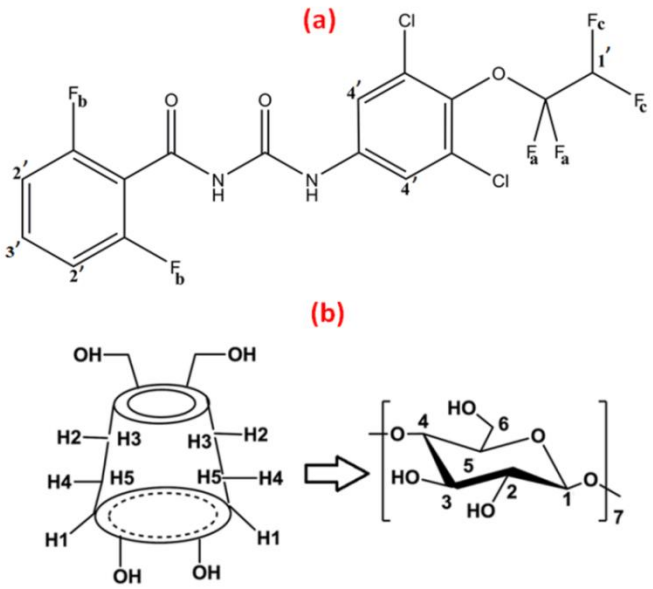

Figure 2.1: Molecular structure of (a) hexaflumuron (HFM) and (b) β-cyclodextrin (β-CD).

It exhibits extremely poor aqueous solubility that can lead to facile accumulation in water or soil, causing rapid poisoning of the environment. Hence effective removal of HFM from environment is a matter of concern. Since there is a possibility that CD may encapsulate HFM resulting in better aqueous solubility, it can act as a scavenging agent for HFM. Here we have made an attempt to understand interaction of HFM with β-CD (structure shown in figure 2.1(b)) using simple chemical shift titration method along with preliminary analysis of linewidth to showcase that these experimental details can give rise to useful qualitative information related to molecular interaction that further ascertain the need of appropriate quantitation using relaxation or diffusion analysis. Figure 2.2 (i and ii) provides representative ^{1}H and ^{19}F NMR spectra of HFM in the absence and in the presence of β-CD. In case of the ^{1}H spectrum of HFM (the peaks are marked with primed numbers) in presence of CD (peaks are marked with non-primed numbers), all the HFM protons are shifted towards high frequency (high ppm values) or low field, indicating possible interaction between HFM and CD. However, the changes in linewidth for any of these peaks are not noticeable. On the other hand, an apparent increase in ^{19}F peak intensities is observed for HFM fluorine peaks with increasing concentrations of β-CD, indicating better aqueous solubility of HFM in the presence of CD. In both, the spectra single sets of HFM ^{1}H and ^{19}F peaks are observed, indicating HFM molecules experiencing fast exchange between free and CD encapsulated state. The changes in ^{1}H chemical shift values for HFM and β-CD on complexation compared to their free form are measured and documented in table 2.1. The maximum chemical shift changes appeared for H1′ followed by H4′ of HFM and H3 (inner cavity proton) of β-CD. The measured shifts in the HFM chemical shift values can be further used to extract quantitative information relevant for the HFM: β-CD complex, namely, the stoichiometry and the binding constant, as discussed in the following sections

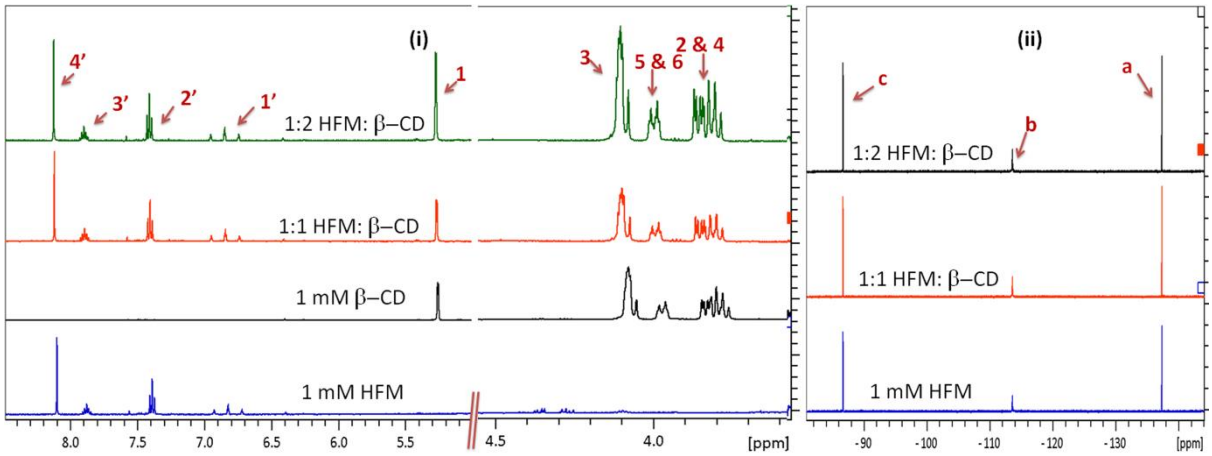

Figure 2.2: (i) ^{1}H NMR spectrum and (ii) ^{19}F NMR spectrum of free β-CD, free HFM, 1:1, and 1:2 HFM: β-CD complex recorded at temperature (T)= 298 K (1' to 4' represents the protons of HFM, 1 to 6 for β-CD protons and a to c for HFM fluorine as shown in molecular structure given in figure 2.1)

Table 2.1: ^{1}H chemical shift difference Δδ ($\delta_{complex}$–δ_{free}) for protons of HFM and β-CD in 1:1 and 1:2 complexed state compared to their free state recorded at 298 K.

Sample	HFM Protons				β-CD Protons			
	Δδ (Hz)							
H:G	H1	H2	H3	H4	H1	H3	H2 & H4	H5 & H6
1:1	11.57	9.45	9.67	11.40	9.82	12.59	9.77	8.13
1:2	12.78	10.18	10.42	12.43	10.85	13.66	10.07	8.80

2.2.2 Determination of stoichiometry: Application of Jobs plot

Jobs plot is a widely used spectroscopic titration method for the determination of stoichiometry of the complex formed between the host (H) and guest (G) [Hirose, 2001; Zhao, et al., 2016]. In the continuous variation method of Jobs plot, the relative proportions of [H] and [G] are varied, keeping the total concentration of added H and G constant, *i.e.* ($[H]_0 + [G]_0 =$ constant) [Renny, et al., 2013; Ulatowski, et al., 2016]. The host-guest complexation phenomena can be determined by monitoring the NMR parameters like chemical shift (δ) or linewidth as a function of the mole fraction of H and G [Upadhyay and Kumar, 2009; R. Zhao et al., 2016]. The changes in chemical shift ($\Delta\delta = \delta_{complex} - \delta_{free}$) are plotted either against guest ($r(G)$=[G]/[G]+[H]) or host ($r(H)$=[H]/[G]+[H]) mole ratio where the total number of moles are kept constant [Cruz, et al., 2008]. It is observed that the concentration of the complex formed will be the highest at the particular mole ratio where the maximum of the curve appears. Hence, the stoichiometry [H_mG_n] of the complex formed can be interpreted from the corresponding mole ratio by identifying the peak of the curve. The simplicity and power of the Job's Plot are compelling, but few limitations are also associated with this plot [Renny et al., 2013; Ulatowski et al., 2016]. The plot becomes less reliable in cases of aggregation of host or guest molecules in solutions or where more than one type of complexes is formed in the system [Loukas, 1997].

The continuous variation Jobs method discussed above is employed to determine the stoichiometry of the complex formed between the host (β-CD) and guest (HFM) [Soni, et al., 2014]. Ten samples are prepared with guest: host mole ratio varying from 0 to 0.9 keeping the total concentration (H_0+G_0) equal to 10 mM. Figure 2.3 (a & b) depicts the changes in ^{1}H

chemical shift ($\Delta\delta = \delta_{complex} - \delta_{free}$) as a function of mole ratio of β–CD (r = [β–CD]/[HFM]+[β-CD]) for HFM protons and β-CD protons respectively. In the case of HFM, the plot showed the maximum shift at 0.3, while for β-CD, the maximum is at 0.6. In agreement with the literature, a plot of such nature indicates formation of complex of 1:2 or 2:1 stoichiometry [Soni et al., 2014]. It thereby suggests that two molecules of β-CD are binding to each HFM yielding a 2:1 stoichiometry of host: guest complex. The plot maxima also revealed that H1′ and H4′ of HFM and H3 of β-CD experienced maximum changes in chemical shift. This observation most probably indicates the preferable mode of insertion of HFM through the aliphatic fluorinated moiety attached to the chlorinated aromatic ring into the CD cavity from the narrower rim side of the β-CD. However, to confirm the mode of insertion, one would definitely require more elaborate NMR experimental analysis employing magnetization transfer methods.

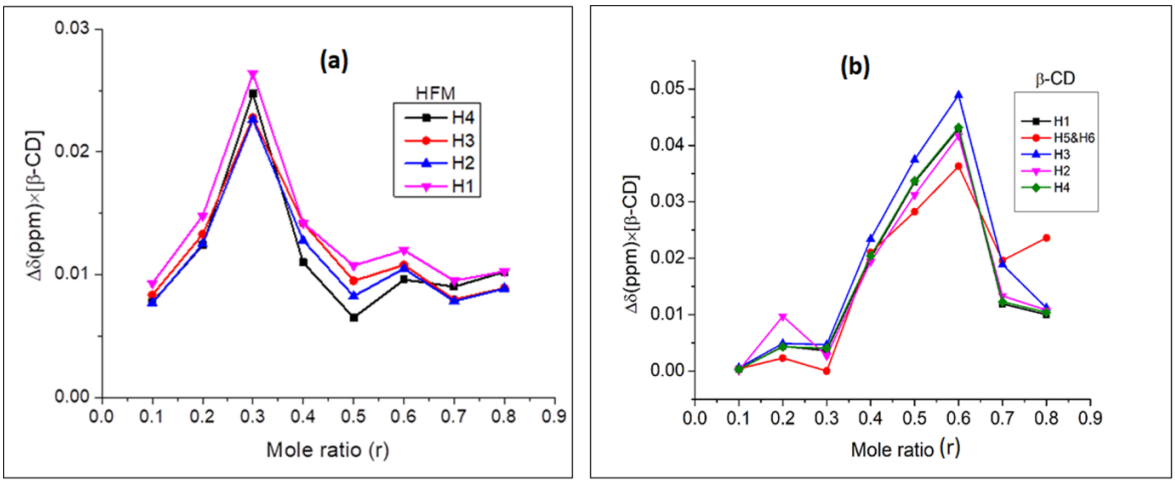

Figure 2.3: Jobs plot analysis for (a) HFM and (b) β-CD protons to determine stoichiometry of the complex.

2.2.3 Determination of Binding Constant: Application of Benesi-Hildebrand Plot

There have been various methods developed in the literature to determine the extent of binding between H and G complexes by correlating the changes in the physical parameters (e.g., NMR chemical shift or linewidth) as a function of H or G concentration. Scott's Plot (equation 2.1) is generally taken into account for determining the binding strength for the H–G complexes with 1:1 stoichiometry in terms of association constant (K_A) [Scott, 1956; Thordarson, 2011].

$$\frac{[G]}{\Delta\delta_{obs}} = \frac{[G]}{\Delta\delta_{\max}} + \frac{1}{K_A\Delta\delta_{\max}} \quad \text{.....(2.1)}$$

Non-binding interactions can also be probed in terms of K_A or equilibrium constant using similar linear double reciprocal Benesi-Hildebrand [B-H] plot. The relevant B-H binding isotherm equation is given as equation 2.2 [Churchill et al., 2006]

$$\frac{1}{\Delta\delta} = \frac{1}{\Delta\delta_{\max}} + \frac{1}{K_A\Delta\delta_{\max}[G]} \quad \text{.....(2.2)}$$

In both the equations, [G] represents the concentration of the guest molecule, $\Delta\delta_{max}$ is the maximum change in the chemical shift for the completely bound host, $\Delta\delta$ is the observed change in chemical shift for H in the presence of G. The ratio of intercept to the slope of the linear B–H plot between $1/\Delta\delta$ and $1/[G]$ can manifest the value of K_A.

The B-H plot for β-CD and HFM complex shown in figure 2.4 (a) did not appear as a straight line, further confirming that the complex does not have a simple 1:1 stoichiometry [Soni et al., 2014]. Therefore, a modified B-H plot between [G]/δ versus $1/[H]^n$ as per equation 2.3 is

analyzed to determine K_A of the complex formed [Meenakshi, et al., 2015; Wen, et al., 2004]. Figure 2.4 (b) provides a representative plot of the modified B-H equation.

$$\frac{[G]}{\delta} = \frac{1}{K_A \alpha [H]^n} + \frac{1}{\alpha} \quad \text{.....(2.3)}$$

where, [G] is the concentration of guest HFM, [H] is the concentration of host β-CD, δ is the chemical shift of complex, a is constant, n is the number of host molecules per guest molecule, and K_A is the association constant for H–G complex.

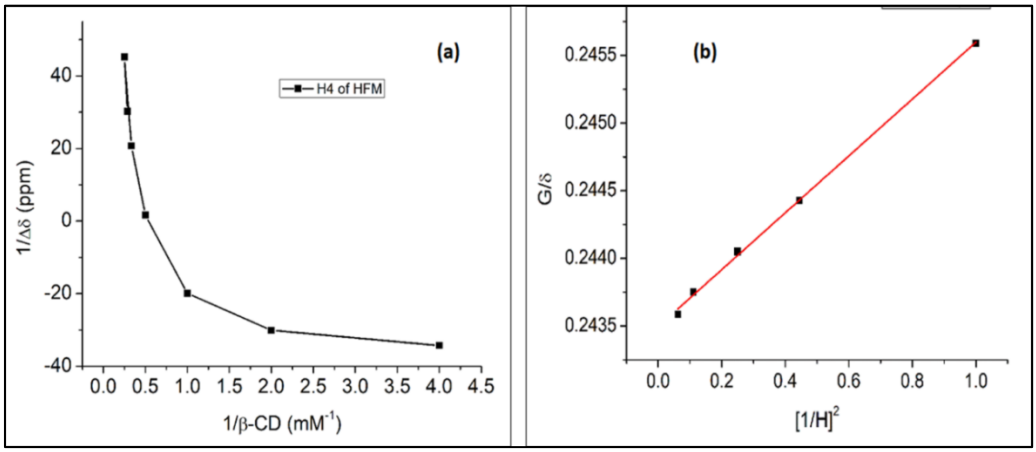

Figure 2.4: Representative (a) B-H plot and (b) modified B-H plot for H4 protons of HFM to determine K_A. Symbols (filled square) represent the experimental data. Plot (a) did not fit linearly with equation 2.2. In plot (b), solid line represents the fitting of experimental data by equation 2.3.

For n=2, the plot results in a perfect straight line as expected for a 2:1 stoichiometric complex. The average K_A was found to be 10.8 M^{-1}, indicative of a weaker interaction between guest and host molecules. The stoichiometry and association constant of the complex have been determined by using ^1H chemical shift titration only as the changes in ^{19}F chemical shift are considerably less compared to ^1H chemical shift. As a concluding remark, it must be mentioned that the changes observed for NMR parameters of HFM in presence of β-CD are minimal, suggesting extremely weak non-bonded interaction leading to very fast chemical exchange between the free and encapsulated state of HFM. Hence, β-CD may not serve as a feasible scavenging agent for HFM, and one should search for other modified cyclodextrin that can possibly offer better encapsulation for HFM.

The perturbations in ligand chemical shift induced due to their significant interaction with the large target are relatively minor compared to the changes in the linewidth. Hence, most of the interaction studies based on the ligand detected NMR methods focus on NMR parameters like NMR relaxation, diffusion coefficient, NOE, etc. [Fielding, 2007; Maity, et al., 2019; Price, 2003]. A brief discussion on these parameters used in context to the current Thesis can be found in the following sections.

2.3 *RELAXATION: THEORETICAL ASPECTS*

NMR relaxation based methods are the efficient and widely preferred tool to probe intermolecular interactions and dynamics in the solutions [Bonechi, et al., 2011; Dubois and Evers, 1992; Kemple, et al., 1997; Kumar, et al., 2003; Martini, et al., 2008; Stockman and Dalvit, 2002]. Relaxation phenomena are generally described as how quickly the non-equilibrium

macroscopic nuclear magnetization generated due to a radiofrequency perturbation restores back to the equilibrium Boltzmann distribution [Keeler, 2002]. The return of nuclear spin magnetization towards its equilibrium state via the exchange of energy between nuclear spins and surroundings is generally characterized by the relaxation rates (inverse of relaxation time).

The interaction between nuclear spins and their surroundings influences the population distribution of the various energy states (ground and excited) of nuclear spin besides generating random fluctuating magnetic fields at the nuclear site. Further, the random thermal motions of the nuclei in solution also provide source of fluctuating local magnetic fields. These fluctuations provide possible pathways for different relaxation processes [Becker, 2000; Farrar and Becker, 1971]. Figure 2.5 shows the four possible energy levels for two spin-1/2 systems (I and S) connected to each other by relaxation induced transition probabilities. W_1 (relaxation process involving flip of either I and S spin), W_0 (both spin flip in the opposite direction) and W_2 (both spin flip in the same direction) are the rate constants for the transition between different energy levels.

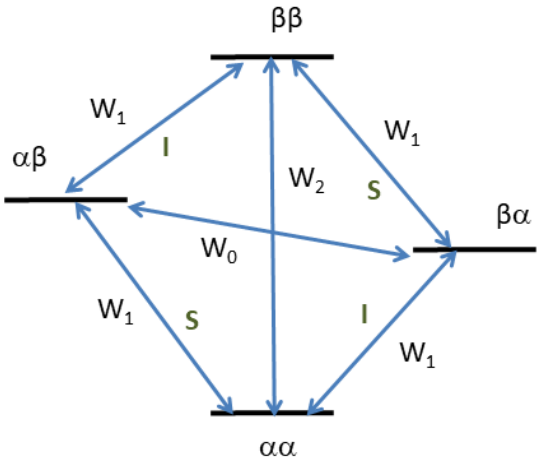

Figure 2.5: Energy level diagram associated with two spin-1/2 systems at thermal equilibrium showing spin states and all the relaxation transition probabilities. W_i indicates the probability of zero, single and double quantum relaxation transitions as indicated by the subscripts.

Various relaxation mechanisms (nuclear spin interactions with the surrounding) in solution state are responsible to make these transitions effective. These relaxation mechanisms are due to i) nuclear dipole-dipole interaction, ii) chemical shift anisotropy (CSA), iii) quadrupolar interaction involving quadrupole moment of the nuclei with the electric field gradient at the nuclei, iv) scalar relaxation, v) spin rotation, and vi) cross-correlation among these different relaxation mechanisms [Slichter, 1989]. In the following, the principal mechanisms, namely, nuclear dipole-dipole interaction and CSA contributing to the relaxation of ^{19}F spins in the solution state, have been discussed briefly along with the definition of the spectral density function and molecular correlation time. It is to be mentioned here that spin rotation of the $-CF_3$ moiety present in any fluorochemical can also contribute to the fluorine relaxation. All the measurements in the current Thesis have been made at room temperature that reduce the possibility of any interference in relaxation by such spin rotation [Kumar et al., 2003; Lambert and Simpson, 1985]. The discussion of the other relaxation mechanisms, namely quadrupole interaction and cross-correlated relaxation etc., is beyond the scope of the present Thesis and will not be addressed further.

(i) Spectral density and correlation time:

Spectral density function plays an important role in understanding relaxation theory. In simple words, spectral density function encompasses the possible gamut of frequencies related to the local fluctuations available in the solution for nuclear energy dissipation. It is a frequency function *(J(ω))* obtained after the Fourier transform of the motional correlation time function *(C(τ))* as expressed in equation 2.4 [Rule and Hitchens, 2006].

$$J(\omega) = \int_{-\infty}^{\infty} C(\tau) e^{-i\omega\tau} d\tau \text{.....(2.4)}$$

(C(τ)) reflects the time-dependent correlation of any parameter value at time t and at (t+*τ)* time. For example, it can be expressed as equation 2.5 for a random Markovian process [Chandrakumar, 1979; Neuhaus and Williamson, 2000; Slichter, 1989].

$$C(\tau) = C(0) e^{-|\tau|/\tau_C} \text{.....(2.5)}$$

Here, τ_c is a critical time that defines the characteristic decay of the correlation function, $C(0)$ is correlation time function at τ=0. The value of $C(\tau)$ decays to zero above this time ($\tau >> \tau_c$) for a particular system. This critical time is termed as the "correlation time" (τ_c). It is roughly the time taken by the particle to rotate 1 radian about it's own axis. In simple words, it is the average time between two successive collisions. In the case of relaxation, τ_c defines the time scale of local field fluctuations by such random molecular motion. This parameter can vary as the function of the solution viscosity, molecular weight, pH, temperature, and other factors such as hydrogen bonding, etc. The correlation time basically summarizes and characterizes the dynamics of molecular motions. Large molecules with high molecular weight will have longer τ_c value as they possess sluggish or slower motion in solution compared to small molecules [Derome, 1987]. Spectral density thereby can be understood as the dependence of the transitional probability of relaxation on the molecular motions at a particular frequency. The corresponding solution of equation 2.4 is given in equation 2.6 [Neuhaus and Williamson, 2000].

$$J(\omega_i, \tau_c) = A\left(\frac{\tau_c}{1+\omega_i^2\tau_c^2}\right) \text{.....(2.6)}$$

Here, A is constant specific for a particular random process and its relative function and ω_i denotes the Larmor frequency of the nuclear spin.

The dependence of the correlation function and the spectral density function of various correlation times is presented in figure 2.6. $C(\tau)$ is a measure of the time evolution of the interaction hamiltonian. And the magnitude of interaction at a particular frequency can be reflected in parameter τ_c.

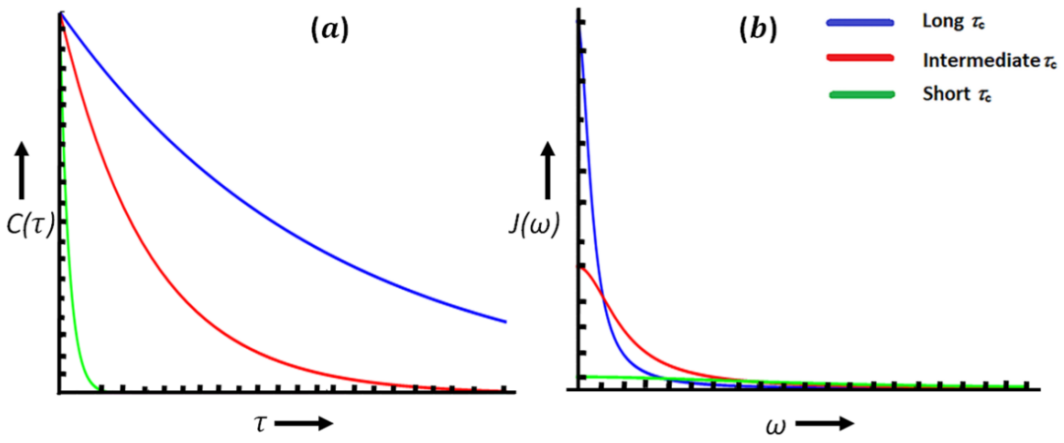

Figure 2.6: Plot presenting schematically the variation of (a) *C(τ)* with τ and (b) corresponding *J(ω)* with frequency at three motional regimes defined by correlation times (τ_c).

Hence, the nature of the curves for $J(\omega)$ is different for the different range of τ_c while the total area under the curve will remain the same.A close inspection of figure 2.6 showed a drastic drop in spectral density function with frequency for longer correlation (slower molecular motion) time. While at shorter correlation time, the amplitude of $J(\omega)$ comparatively remains unchanged for a long-range of frequency. The magnitude of $J(\omega_0)$ is maximal when ω=0 for any value of τ_c [Dey, 2019; Neuhaus and Williamson, 2000]. The relaxation rates corresponding to the relevant relaxation mechanisms can be expressed in terms of the spectral density functions given in the following sections as per the semi-classical treatment approach [Wangsness and Bloch, 1953; Redfield, 1965].

(ii) Dipole-Dipole (DD) Interaction:– Interaction between magnetic dipoles is a fundamental mechanism that contributes majorly to the relaxation of spin ½ nuclei in the solution-state. The magnetic field induced by the nuclear spins (as they possess magnetic moment) can interact with the other nuclear spin, causing the spin relaxation. The magnitude of direct dipole-dipole coupling interaction is very large compared to other mechanisms. In the case of fluorinated molecules, one of the most efficient relaxation mechanisms experienced by ^{19}F nuclear spin is dipole-dipole interactions, both heteronuclear and homonuclear in nature; the former with the neighbouring protons while the latter with the fluorine nuclei that surround them [Gerig, 1997]. The dependence of ^{19}F relaxation rates on spectral density function $J(\omega)$ and the corresponding expression for ^{19}F longitudinal relaxation rate (R_1) and transverse relaxation rate (R_2) considering isotropic tumbling of ^{19}F–^{1}H interaction dipole in SI units are given as [Dalvit, 2007]: For distinguishable pair of spins (unlike spins, heteronuclear system);

$$R_1 = \frac{1}{T_1} = \frac{d^2}{10}[3J(\omega_I) + J(\omega_I - \omega_s) + 6J(\omega_I + \omega_s)].....(2.7a)$$

$$R_1 = \left(\frac{\mu_0}{4\pi}\right)^2 \frac{1}{10}\gamma_I^2\gamma_S^2\hbar^2\Sigma\frac{1}{r_{IS}^6}\cdot\tau_c\cdot\left(\frac{3}{1+\omega_I^2\tau_c^2} + \frac{1}{1+(\omega_I-\omega_S)^2\tau_c^2} + \frac{6}{1+(\omega_I+\omega_S)^2\tau_c^2}\right)....(2.7b)$$

$$R_2 = \frac{1}{T_2} = \frac{d^2}{20}[4J(0) + 3J(\omega_I) + 6J(\omega_S) + J(\omega_I - \omega_s) + 6J(\omega_I + \omega_s)]...(2.8a)$$

$$R_2 = \left(\frac{\mu_0}{4\pi}\right)^2 \frac{1}{20}\gamma_I^2\gamma_S^2\hbar^2\Sigma\frac{1}{r_{IS}^6}\cdot\tau_c\cdot\left(4 + \frac{3}{(1+\omega_I^2\tau_c^2)} + \frac{6}{(1+\omega_S^2\tau_c^2)} + \frac{1}{\left(1+(\omega_I-\omega_S)^2\tau_c^2\right)} + \frac{6}{\left(1+(\omega_I+\omega_S)^2\tau_c^2\right)}\right)....(2.8b)$$

$$Here, d^2 = \left(\frac{\mu_0}{4\pi}\right)^2\gamma_I^2\gamma_S^2\hbar^2\Sigma\frac{1}{r_{IS}^6}$$; I and S represents nuclear spin i.e. I = ^{19}F and S = ^{1}H,

For indistinguishable pair of spins (like spins, homonuclear system), R_1 and R_2 can be written as:

$$R_1 = \frac{1}{T_1} = \left(\frac{\mu_0}{4\pi}\right)^2 \frac{3}{10}\gamma_I^4\hbar^2\Sigma\frac{1}{r_{II}^6}\cdot\tau_c\cdot\left(\frac{1}{1+\omega_I^2\tau_c^2} + \frac{4}{1+4\omega_I^2\tau_c^2}\right)....(2.9)$$

$$R_2 = \frac{1}{T_2} = \left(\frac{\mu_0}{4\pi}\right)^2 \frac{3}{20}\gamma_I^4\hbar^2\Sigma\frac{1}{r_{II}^6}\cdot\tau_c\cdot\left(3 + \frac{5}{(1+\omega_I^2\tau_c^2)} + \frac{2}{(1+4\omega_I^2\tau_c^2)}\right)....(2.10)$$

Here, I is either ^{19}F or ^{1}H; $\hbar$: reduced Planck's constant; μ_0: permeability of free space; γ_i: gyromagnetic ratio of the i-th spin; τ_c: molecular correlation time; r_{II}: internuclear distance between I and I nuclei; r_{IS}: internuclear distance between I and S nuclei. T_1 and T_2 are the longitudinal and transverse relaxation time, respectively.

Figure 2.7 represents the logarithmic plot for the ^{19}F relaxation rate as a function of correlation time simulated using equation 2.7 and 2.8 for the heteronuclear (^{19}F–^{1}H) case. The simulation is performed for a common fluorinated molecule *i.e.*, fluorobenzene with internuclear distance (r_{HF}) equal to 2.20 Å and ^{19}F Larmor precession frequency of 470.7 MHz [Dalvit, 2007].

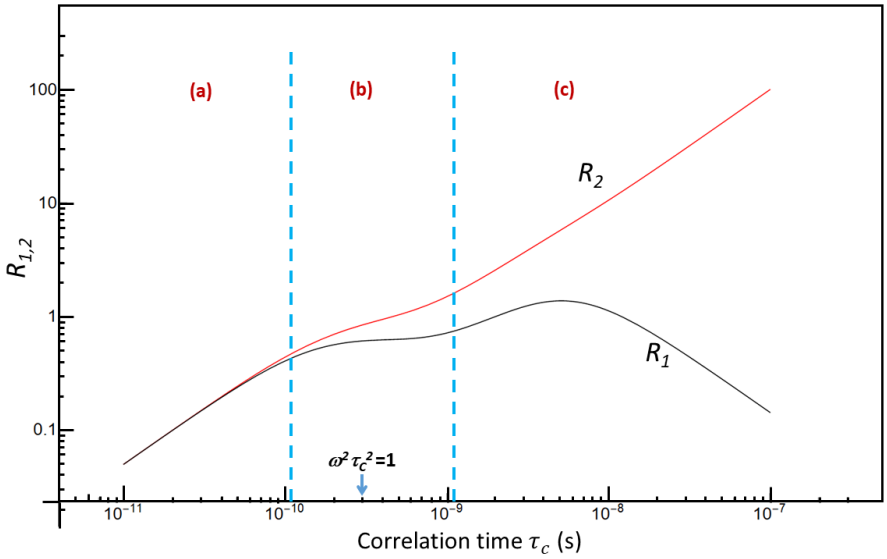

Figure 2.7: Logarithmic plot of ^{19}F R_1 and ^{19}F R_2 as a function of correlation time extracted from equation 2.7 and 2.8 based on dipolar interaction for the heteronuclear system at 470.7 MHz ^{19}F Larmor precession frequency.

The figure 2.7 can be divided into three sections based on the magnitude of τ_c for a fixed value of ω, namely, (a) Extreme narrowing limit (fast motion limit, $\omega^2\tau_c^2<<1$) for small molecules having lower molecular weight (MW) (b) Intermediate motion regime ($\omega^2\tau_c^2=1$) for intermediate MW (c) Spectral diffusion limit (slow-motion limit, $\omega^2\tau_c^2>>1$) for macromolecules having large MW. It can be seen that the R_2 value always showed an increase with increasing correlation time on moving from the region (a) to (c) while R_1 showed a bell-shaped trend. It leads to a minimal change in the ^{19}F R_1 value measured at the various motional regimes. Hence ^{19}F R_2 can be identified as a better and an efficient parameter than ^{19}F R_1 for identifying binding of the ligands to the targets [Dalvit, et al., 2003].

(iii) Chemical Shift Anisotropy (CSA): CSA is the second dominant relaxation mechanism for ^{19}F nuclei in solution. CSA acts as an essential mechanism of relaxation for a set of nuclei with a small magnetic moment and a wide span of chemical shifts like ^{15}N, ^{19}F, ^{31}P, ^{57}Fe, ^{113}Cd, etc. [Becker, 2000]. When magnetic nuclei are placed in an external magnetic field, the electron cloud surrounding the atomic nucleus induces a local magnetic field due to their rotatory motion about the nucleus. This induced local magnetic field alters the magnitude of the applied external magnetic field felt at the site of the atomic nucleus. This effect is known to be the chemical "shielding" or "screening" effect exerted by the electrons and is described by the NMR parameter shielding constant or screening constant. The movement of electrons around the nucleus is highly orientation-dependent and can be more fluent in one direction than the other that causes anisotropy in the shielding parameter and, therefore, in chemical shift [Hazime, et al., 2012]. This orientation-dependent tumbling of the molecule with respect to the magnetic field generates the local field contributing to the relaxation processes. It is not only the net magnetic field that gets altered but also their direction. Hence, CSA can be understood as the function of the orientational motion of a molecule in the presence of magnetic field [Rule and Hitchens, 2006]. Since nine electrons surround ^{19}F compared to one electron of ^{1}H, the anisotropies for ^{19}F are relatively very high compared to ^{1}H (almost negligible in the case of ^{1}H). Anisotropy of the ^{19}F chemical shift contributes significantly to the relaxation (R_1, R_2) of the ^{19}F at higher fields. For a cylindrically symmetric system, ^{19}F relaxation rates due to CSA can be mathematically expressed as follows [Dalvit, 2007]:

$$R_1 = \frac{1}{T_1} = \frac{2}{15}(\sigma_{\parallel} - \sigma_{\perp})^2 \omega_F^2 \tau_c \frac{1}{1+\omega_F^2\tau_c^2} \text{.....(2.11)}$$

$$R_2 = \frac{1}{T_2} = \frac{2}{15}(\sigma_{\parallel} - \sigma_{\perp})^2 \omega_F^2 \tau_c \left(\frac{2}{3} + \frac{1}{2} \frac{1}{\left(1 + \omega_F^2 \tau_c^2\right)} \right) \text{.....(2.12)}$$

Here, $(\sigma_{\parallel} - \sigma_{\perp})$ represent the shielding anisotropy where $\sigma_{\parallel}$ is the shielding parameter when the bond axis of the molecule is oriented parallel to the magnetic field and $\sigma_{\perp}$ when the molecular bond of interest is in a direction perpendicular to the external magnetic field (MF). The other terms have their usual meaning.

The size of CSA can also be represented as a second-order tensor quantity in 3×3 matrix form [Keeler, 2002]. From the expressions, it can be seen that unlike dipole-dipole interaction, CSA varies quadratically with increasing magnetic field B_0. These equations also depict that CSA contribution to ^{19}F R_2 is higher than for the ^{19}F R_1 by a factor of 2/3, causing a greater broadening of ^{19}F linewidth at the higher magnetic field.

Figure 2.8 has been generated by simulating equation 2.11 and 2.12 for a cylindrically symmetric fluorinated molecule fluorobenzene with known CSA parameters [Dalvit, 2007]. It can be seen from the figure that R_2 always increases with τ_c while R_1 initially increases and further decreases. The more considerable changes in R_2 value further contribute to the statement mentioned in the previous section that R_2 can be considered as a more sensitive parameter towards any change in the environment [Dalvit et al., 2003].

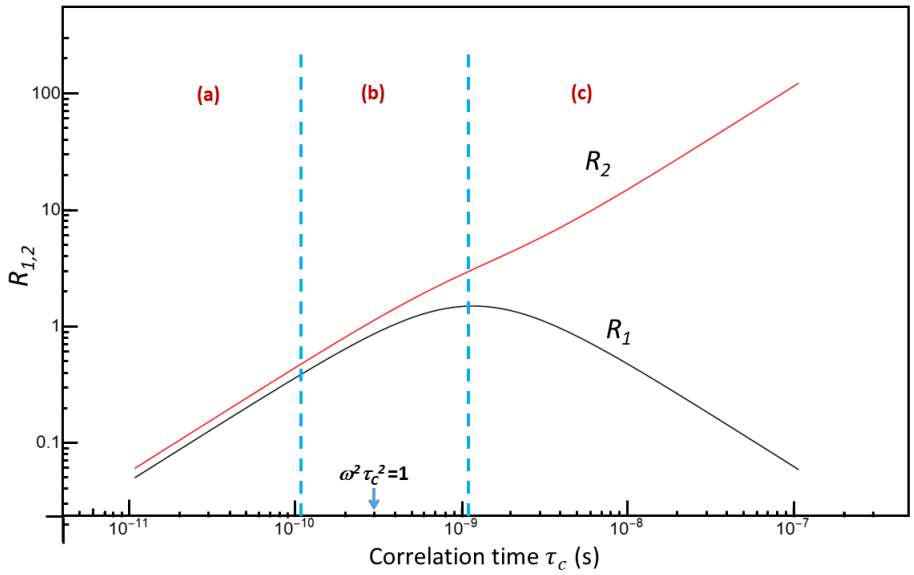

Figure 2.8: Logarithmic plot of ^{19}F R_1 and ^{19}F R_2 as a function of correlation time extracted from equation 2.11 and 2.12 based on chemical shift anisotropy at 470.7 MHz ^{19}F Larmor precession frequency.

Since relaxation rates are additive, the resultant relaxation rate for ^{19}F nuclei will be the sum of respective dipolar and CSA contributions. Further, these two relaxation mechanisms can interfere with each other to generate cross-correlated relaxation processes.

(iv) Cross correlation: Interference effect

Several mechanisms stimulate the relaxation of nuclear spins, as discussed earlier. The simultaneous presence of different relaxation pathways can result in interference between two different relaxation pathways that generates cross terms between these mechanisms. Relaxation of nuclear spins due to such cross terms is known as cross-correlated relaxation (CCR) [Kumar, et al., 2000]. For example, the molecule's overall tumbling motion can change the relative

orientation of DD tensor and CSA interaction tensor with respect to the external magnetic field giving rise to correlated orientational fluctuations [Peng, 2001]. The influence of cross-correlation is generally seen for nuclei with large CSA values like ^{31}P, ^{19}F, ^{15}N, and ^{13}C etc. ^{19}F T_1 measurements using standard spin inversion recovery pulse sequence (discussed later in section 2.4) are employed in literature for the determination of cross-correlation between CSA of fluorine and its dipolar interaction with nearby protons [Elavarasi and Dorai, 2010]. Active cross-correlated relaxation due to ^{19}F CSA and ^{19}F–^{1}H DD interaction can be directly evidenced by monitoring differential or unequal recovery of various inverted lines of a ^{19}F spin multiplet. Various literature reports provide a detailed theoretical analysis of such cross-correlated relaxation by introducing different magnetization modes [Dorai and Kumar, 2001; Elavarasi and Dorai, 2010; Sitkoff and Case, 1998]. However, the description of such an analysis is beyond the scope of the present Thesis. It must be pointed out here that an overall analysis of ^{19}F relaxation at high magnetic field throws number of challenges due to the simultaneous involvement of DD, CSA and CSA-DD cross-correlated relaxation mechanisms. In general, extraction of correlation time for fluorinated molecules from relaxation analysis of ^{19}F becomes a daunting task at high magnetic field. The scenario changes while working at a considerably lower magnetic field. The following section details the relaxation behaviour of ^{19}F nuclei at a lower magnetic field *ca.* 0.34 T; the one that has been employed in the current Thesis.

2.3.1 Fluorine relaxation at low field (0.34 T)

High magnetic field leads to higher sensitivity and higher resolution for NMR spectra but are not optimal for all NMR applications, neither for all nuclei. Different relaxation pathways influence the relaxation phenomenon at higher fields with reasonable magnitude and hence cannot be ignored. It also makes the analysis of relaxation data complex and cumbersome as various intra and intermolecular effects have to be considered [Charlier et al., 2013; Kadeřávek et al., 2019; Kumar et al., 2003]. However, acquisition of NMR data at the lower magnetic field (taking the example of ^{19}F in specific at 0.34 T) offers certain specific advantages over the high field:

(a) Mitigation of CSA: The contribution in relaxation rates due to mechanisms like CSA generally increases quadratically with magnetic field strength. At a considerably lower magnetic field, the magnitude of CSA becomes small enough to be neglected reducing the complexity of relaxation rate expressions since the corresponding relaxation rate is proportional to the square of the Zeeman field (B_0). For example, in the present Thesis, the measurements made at 0.34 T [13.7 MHz (^{19}F)/ 14.6 MHz (^{1}H)] reduces the CSA by three orders of magnitude as compared to that at 11.76 T [470.7 MHz (^{19}F)/ 500 MHz (^{1}H)], *i.e.*, nearly 1200 fold mitigation of CSA effect as demonstrated below with a simple calculation.

$$\frac{[\omega_{F(11.7T)}]^2}{[\omega_{F(0.34T)}]^2} = \frac{2\pi[\nu_{F(11.7T)}]^2}{2\pi[\nu_{F(0.34T)}]^2} = \frac{(470.7)^2}{(13.7)^2} = 1180 \sim 1200$$

(b) Extreme narrowing condition: Very low fields such as 0.34 T used in the current Thesis fulfils the extreme narrowing condition, *i.e.*, $4\omega^2\tau_c^2 \ll 1$ (for homonuclear case) remaining maintained for a broad range of correlation times that covers a time scale spanning over three orders of magnitude. For example, for ^{19}F containing molecule with rotational correlation times (τ_c) of 500 ps and 50 ps at 0.34 T [13.7 MHz (^{19}F)], the value of $4\omega_F^2\tau_c^2$ will come out to be:

$$4\omega_F{}^2\tau_c^2 = 4\times(2\pi\times13.7\times10^6)^2\times(500\times10^{-12})^2 = 0.007 \sim 0.010 \ll 1$$

$$4\omega_F{}^2\tau_c^2 = 4\times(2\pi\times13.7\times10^6)^2\times(50\times10^{-12})^2 = 0.00007 \sim 0.0001 \lll 1$$

(c) Simplification of relaxation rate expression: The above two points lead to simplication of the relaxation rate expression at low field. Equations 2.13 and 2.14 represent the ^{19}F relaxation rate for homonuclear (^{19}F–^{19}F) and heteronuclear (^{1}H–^{19}F) cases under extreme

narrowing conditions at the low field expressed in SI units as [Abragam, 1961; Solomon, 1955]:

$$R_{1FF} = \left(\frac{1}{T_{1FF}}\right) = \frac{3}{10}\left(\frac{\mu_0}{4\pi}\right)^2 \gamma_F^4 \hbar^2 \Sigma \frac{1}{r^6_{F-F}}\left(5\tau_c\right) \text{....(2.13)}$$

$$R_{1FH} = \left(\frac{1}{T_{1FH}}\right) = \left(\frac{\mu_0}{4\pi}\right)^2 \gamma_F^2 \gamma_H^2 \hbar^2 \Sigma \frac{1}{r^6_{F-H}}\left(\tau_c\right) \text{....(2.14)}$$

These two expressions instantly simplify the inference of τ_c as τ_c can be easily extracted from the experimentally measured R_1 values using equation 2.13 and 2.14 where all the other parameters are known. Therefore, relaxation measurements at low magnetic fields provide rich information on molecular dynamics upto nanoseconds time scale as it fulfils the extreme narrowing condition upto τ_c that is as long as hundreds to thousands of ps. For example, for ^{19}F–^{1}H heteronuclear case at 0.34 T [13.7 MHz (^{19}F)/ 14.6 MHz (^{1}H)] following extreme narrowing limit (considering $4\omega^2\tau_c^2$=0.01), τ_c comes out to be ~552 ps.

$$(\omega_F + \omega_H)^2 \tau_c^2 = 0.01$$

$$(2\pi\nu_F + 2\pi\nu_H)^2 \tau_c^2 = 0.01$$

$$\tau_c = 552\, ps$$

2.4 MEASUREMENT OF RELAXATION TIME: EXPERIMENTAL SETUP

Longitudinal or spin-lattice relaxation time (T_1) characterizes the recovery of nuclear spins in a direction parallel to the static field (z-direction) while transverse or spin-spin relaxation time (T_2) constant accounts for the decay of magnetization in the direction normal to the applied static field. Both the relaxation processes are usually exponential in nature and are modelled as first-order rate processes [Farrar and Becker, 1971; Wolf, 1979]. Felix Bloch proposed a set of phenomenological equations for a group of physically non-interacting spins that represents the time evolution of nuclear magnetization (M), considering relaxation as an essential process of magnetization decay characterized by respective time constants. Equations 2.15 and 2.16 represents the time derivative of both longitudinal and transverse magnetization components [Bloch, et al., 1946; Wangsness and Bloch, 1953]:

$$\frac{dM_z}{dt} = \gamma(M \times B)_z - \frac{\left(M_z - M_0\right)}{T_1} \text{.....(2.15)}$$

$$\frac{dM_{y/x}}{dt} = \gamma(M \times B)_{y/x} - \frac{\left(M_{y/x}\right)}{T_2} \text{.....(2.16)}$$

Here, T_1 describes the time taken for the return of M_z (magnetization vector in the z-direction) to equilibrium magnetization along the magnetic field (M_0). T_2 accounts for the decay of M_x/M_y (magnetization vector in the x- and y-direction) to zero. B is the applied magnetic field.

Equation 2.17 and 2.18 provides the solutions of this set of Bloch equations that are obtained after application of an appropriate RF pulse and with an assumption that the relaxation phenomena are best described as first-order processes [Becker, 2000]:

$$M_z(t) = M_0(1 - 2e^{(-\tau/T_1)}) \text{.....(2.17)}$$

$$M_{x,y}(t) = M_0 \exp^{(-\tau/T_2)}) \text{.....(2.18)}$$

Figure 2.9 (a, b, and c) represents the standard inversion recovery pulse sequence employed in the current Thesis for ^{19}F and ^{1}H T_1 measurements [Freeman et al., 1974]. Figure 2.10 (a, b, and c) represent standard CPMG pulse sequence proposed by Carl, Purcell, Meiboom, and Gill for ^{19}F and ^{1}H T_2 measurements [Carr and Purcell, 1954; Meiboom and Gill, 1958]. In the figures 2.9 and 2.10, τ_m represents the recovery delay, τ is spin-echo time and n indicates the loops of spin-echo sequence ($\tau/2$ – π pulse – $\tau/2$). Relaxation times T_1 and T_2 are extracted by

plotting the measured experimental signal intensities as a function of the recovery period (τ_m) and spin-echo loop, respectively. A nonlinear least-squares fitting procedure is used following equation 2.17 and 2.18 based on the Levenberg-Marquardt algorithm [Marquardt, 1963].

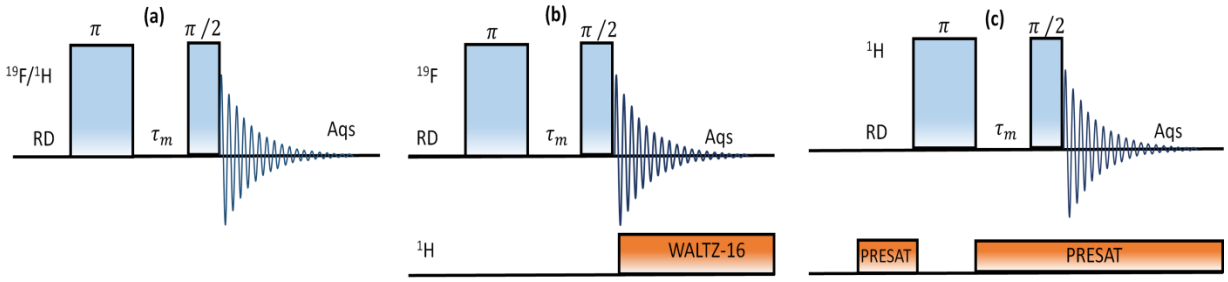

Figure 2.9: Inversion recovery pulse sequence for measuring (a) ^{19}F (^1H coupled) *T1* or ^1H T_1 (b) ^{19}F(^1H decoupled) T_1 (c) ^1H T_1 (solvent suppressed); τ_m: recovery delay; RD: relaxation delay; Aqs: acquisition time; rectangular blue bars are hard pulse 90° and 180° pulses; orange bars: presaturation and decoupling scheme.

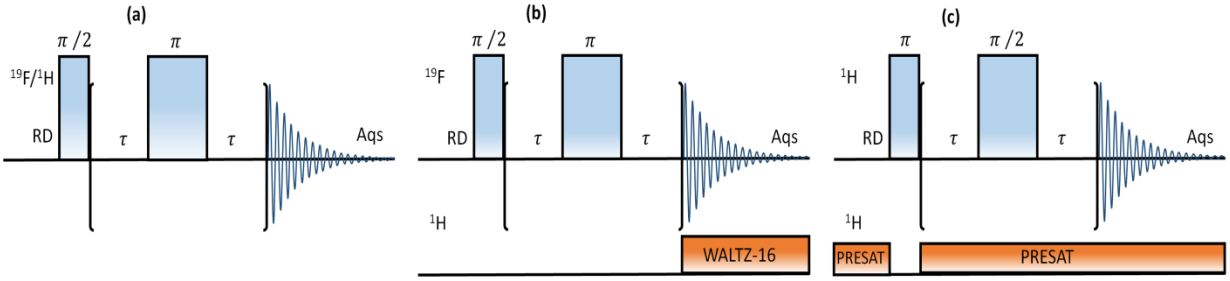

Figure 2.10: CPMG Pulse sequence for measuring (a) ^{19}F (^1H coupled) T_2 or ^1H T_2 (b) ^{19}F (^1H decoupled) T_2 (c) ^1H T_2 (solvent suppressed); 2τ: echo time; RD: relaxation delay; Aqs: acquisition time; retangular blue bars: hard 90° and 180° pulses; orange bars: presaturation and decoupling scheme.

2.5 DIFFUSION NMR: SELF-DIFFUSION COEFFICIENT

Molecules in solutions are in constant random (Brownian) motions – a molecular behaviour more formally known as translational diffusion. This process is the underlying mechanism of mass transport and corroborates most chemical processes [Evans, 2020]. NMR provides an array of extremely well-established methods employing pulse field gradients (PFG), allowing quantification of molecular self-diffusion coefficient (D) – the parameter conventionally describing motions of molecules in the solution. D can be defined as a parameter known to characterize mean displacement of the diffusing molecules (translation motion) in solutions and is characteristic of the molecular species present in solution [Augé et al., 2009]. Various physical and chemical properties such as molecular size, pH, temperature, and the viscosity of the solution can alter the value of D [Stilbs, 1999]. The relation of D with these above mentioned parameters can be described by Stoke-Einstein's relation given in equation 2.19 [Johnson, 1999].

$$D = \frac{k_B T}{6\pi\eta r_H} \quad \text{.....(2.19)}$$

Here, k_B = Boltzman constant, T = Temperature, η = viscosity, r_H = hydrodynamic radius that can be related to molecular size.

Measurement of the self-diffusion coefficient offers an extremely reliable technique to decipher molecular interaction and association in solution. When a fast moving small molecule interacts with a macromolecule or supramolecular system or undergoes aggregation, its mobility slows down proportionately with its molecular size and weight. Consequently, a considerable change in the *D* value of the small molecule can be experimentally detected. Hence, diffusion NMR provides a fair means of quantifying molecular aggregation, solvation, and binding of the ligand to the target by evaluating the change in their *D* values [Derrick, et al., 2002; Liu, et al., 1997; Lucas and Larive, 2004; Luo, et al., 1999; Šmejkalová and Piccolo, 2008a, 2008b; Wimmer, et al., 2002]. Ligand diffusion coefficient (*D*) measured for the ligand-target complex can reflect the binding affinity as well [Price, et al., 2002; Zhuang et al., 2013a, 2013b].

A number of PFG based pulse sequences are discussed in the literature for determining *D*. Stejskal and Tanner have first proposed the simplest PFG approach based on stimulated spin-echo (STE) for measuring *D* [Stejskal and Tanner, 1965]. PFG diffusion NMR pulse sequences such as STE [Tanner, 1970], PGSE (Pulsed-Gradient spin-echo) [Stejskal and Tanner, 1965], BPPSTE (Bipolar Pairs stimulated echo), LED (Longitudinal Eddy Current), BPPLED (Bipolar Pairs Gradient LED) [Wu, et al., 1995], CPMG-BPPSTE (CPMG modified BPPSTE), and GOSE-BPPSTE (Gradient modified spin echo-BPPSTE) [Otto and Larive, 2001], etc. have been comprehensively reviewed in terms of their advantages and limitations by Lucas et al. [Lucas et al., 2002]. Generally, all these sequences employ magnetic field gradients (z-axis) with spin-echo pulse sequence known as the pulsed field gradient echo to spatially label the positions of the nuclear spins within the NMR tube as shown in figure 2.11. The first gradient is applied during the first dephasing period to encode the nuclear spins spatially. Further, for the spatially decoding of the nuclear spins, the second gradient of equal strength is applied after the spin-echo refocusing pulse. The spins that have not been displaced from their original positions will impart to the spin-echo only while the spins that have moved far away will not contribute to the NMR signal [Karlicek and Lowe, 1980]. Hence, it is possible to determine *D* by changing the gradient duration (δ) or strength (*G*).

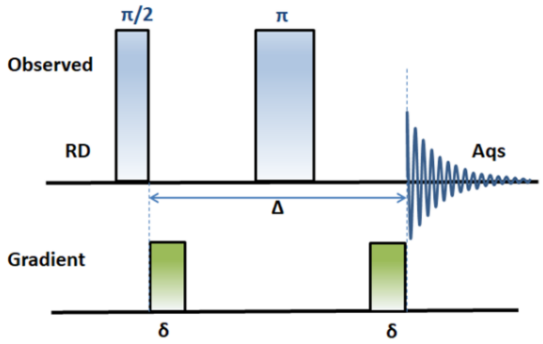

Figure 2.11: Pulse sequence showing basic pulsed gradient spin echo widely used in diffusion NMR pulse sequences. Blue bars represent the RF pulses, and green bars are gradient pulses. δ: gradient length; Δ: diffusion delay; RD: relaxation delay; Aqs: acquisition time. The magnetization is excited with a π/2 RF pulse and then dispersed using a magnetic field gradient pulse. After a period of Δ/2, a π RF pulse inverts the dispersed magnetization such that after a period of Δ the magnetization is the negative of what it was following the gradient pulse. At this point, a second gradient pulse is applied to refocus the signal.

The presentation of diffusion NMR spectra are often done in two-dimensional format for better visualization and easy qualitative interpretation known as diffusion ordered spectroscopy (DOSY). DOSY is the resultant representation of the diffusion spectra obtained by incrementing the areas of the gradient pulses in PFG-NMR and transforming the NMR signal amplitudes with

respect to the square of the area of gradient pulses [Johnson, 1999]. In DOSY spectra, the chemical shift information of the species is represented in one dimension, and the other dimension represents the diffusion coefficients of the respective species. The DOSY spectra exhibit the summary of diffusion results as a graphical overview [Evans, 2020]. It can be used to differentiate various components of a mixture based on a particular component signal and an associated *D* value that further depends on the size, as mentioned earlier.

In the present Thesis, the BPPLED pulse sequence shown in figure 2.12 that incorporates pulse field gradient has been employed to determine the ligand self-diffusion coefficient in the presence and absence of the target.

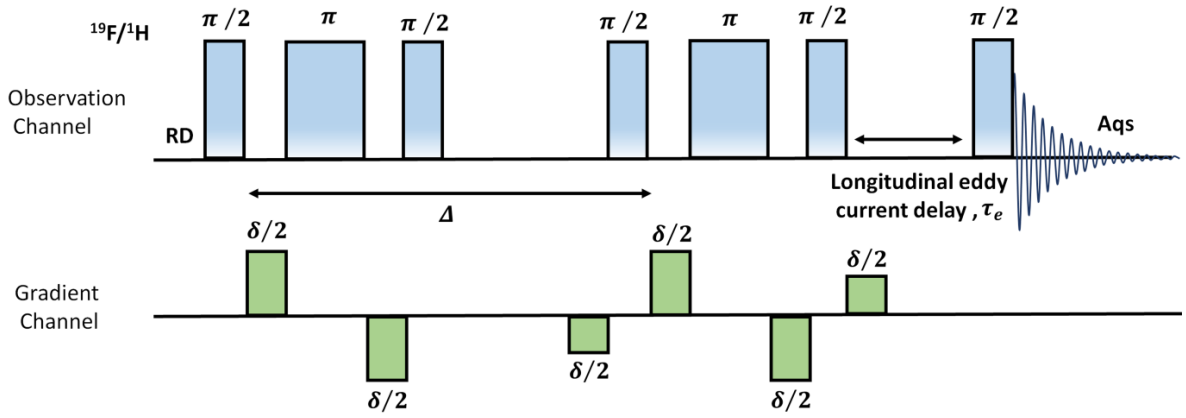

Figure 2.12: Pulse sequence for diffusion coefficient measurement (BPPLED sequence). Blue bars represent the RF pulses and green bars are gradient pulses. RD: relaxation delay; Aqs: acquisition time; δ: gradient length and Δ : diffusion delay.

BPPLED (bipolar–pair pulse sequence with longitudinal eddy current delay) is known for being more efficient than other existing diffusion pulse sequences. It enables a more accurate determination of the self-diffusion coefficient [Derrick et al., 2002]. Bipolar pulses (BP), a pair of gradients of equal magnitude but opposite sign separated by π pulse, are used to refocus the chemical shift evolution during encoding and decoding time and thereby diminishing any modulation by the chemical exchange [Wu et al., 1995]. It also eliminates the artefacts related to eddy current and static gradients [Lucas and Larive, 2004]. In this method, a series of spectra are acquired with increasing gradient strength and keeping Δ and δ values constant (pseudo-2D format). In the present case, the maximum gradient strength is 51 G/cm and is calibrated for water ($D=2.29\times10^{-9}$ m^2s^{-1}) at 298K [Luo et al., 1999]. The apparent diffusion coefficient *D* is further extracted by fitting the experimentally determined attenuated signal intensities as a function of increasing gradient strength (G) using equation 2.20.

$$I = I_0 \exp\left[-D(G\delta\gamma)^2(\Delta - \delta/3)\right] \quad .....(2.20)$$

Here, I and I_0: intensities in the presence and absence of gradient pulses, respectively, γ : the gyromagnetic ratio, δ: gradient length, Δ: diffusion delay, G: gradient strength, and D: apparent self-diffusion coefficient.

To analyse the binding affinity of a ligand to a macromolecule using the experimentally measured *D* of the ligand, one needs to consider the effect of an ongoing chemical exchange between the free and the bound state of the ligand. Under fast reversible exchange conditions on diffusion time scale (~100ms), the experimentally observed diffusion coefficient of the ligand is a

weighted average value of the ligand diffusion coefficient in its free and bound state as represented by equation 2.21 [Wimmer et al., 2002].

$$D = (1 - P_b)D_F + P_b D_B \text{.....(2.21)}$$

Here, D: Observed ligand diffusion coefficient (weighted average of D_F and D_B), D_B: Diffusion coefficient of the fully bound ligand; at a very low concentration of ligand D can be well approximated to be the diffusion coefficient of the free target *i.e.,* protein or humic acid in present Thesis (D_B); D_F: Diffusion Coefficient of free ligand, P_b: bound ligand population/fraction. P_b can be further related to binding constants (K_D or K_A), enabling the determination of binding strength of the ligand-target complex. The respective expressions for binding constants are discussed in forthcoming chapters.

2.6 MAGNETIZATION TRANSFER BASED METHODS

Direct magnetic interactions between nuclear dipoles located close to each other in space result in dipolar coupling. These time-dependent dipolar couplings provide an important source of nuclear relaxation in solution. The direct through-space interactions between nuclei provide incoherent magnetization transfer pathways through cross-relaxation known as nuclear Overhauser effects (NOEs). Experimental observation of the NOE is realized by monitoring the change in signal intensity of a spin after the perturbation of a nearby spin with radio-frequency irradiation. The rate constants governing cross-relaxation depend on the spatial distance between the two nuclei and the rotational mobility of the vector connecting the two atoms. NOEs are sensitive probes of short-range, through-space, intramolecular, and intermolecular interactions because the NOE intensity falls off rapidly with increasing distance ($1/r^6$). As such, the NOE provides relative spatial information for structure determination and allows the use of solution NMR to examine the interactions between nuclei that are not necessarily covalently bound but are within five angstroms of each other [Skinner and Laurence, 2008]. Various methods rely on the principle of NOE and are used to probe ligand-target interactions such as heteronuclear NOE, STD (saturation transfer difference), ODNP (Overhauser dynamic nuclear polarization), INPHARMA (interligand NOE for Pharmacophore Mapping), transferred NOE, ILOE (intramolecular ligand-ligand NOE), Water-LOGSY (water ligand observed through gradient spectroscopy), cross-saturation and transferred saturation, etc. [Maity et al., 2019]. STD and ODNP have been employed in the current Thesis work to investigate molecular systems and are specifically discussed in the following sections.

2.6.1 Saturation transfer difference (STD): Group epitope mapping

Saturation Transfer Difference (STD) NMR is one of the most well-established and efficient ligands detected techniques for addressing weak non-covalent interaction between small molecules and macromolecular targets [Viegas, et al., 2011; Wang, et al., 2004]. This method was first introduced in literature by Mayer and Meyer and involved transferring through-space nuclear polarization from the target to the ligands bound to the target via intermolecular dipole-dipole interaction (cross-relaxation) between ligand and target [Mayer and Meyer, 1999]. Acquisition of the STD NMR spectrum requires recording of two different experiments one with target NMR active nuclei saturated with an appropriate radiofrequency pulse (STD_{on}) and the other experiment is carried out without the saturation pulse or with the saturation pulse applied far away from the target as well as ligand resonances (STD_{off}). The latter experiment is in principle, similar to a single pulse excitation spectra of the target and ligand. Figure 2.13 represents a pictorial depiction of the principle of STD.

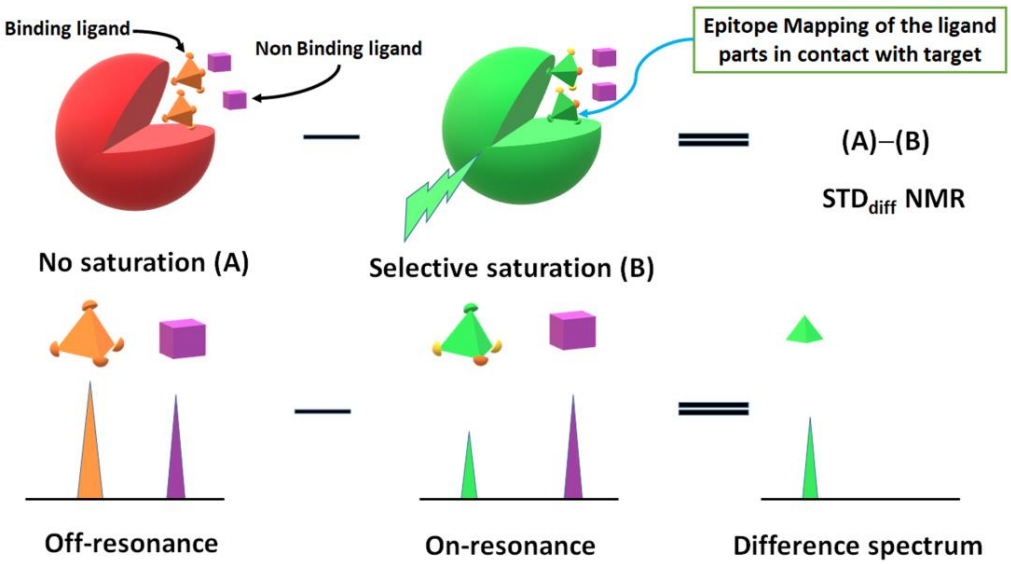

Figure 2.13: Pictorial Scheme exhibiting STD NMR mechanism for the ligand-target system [Mayer and Meyer, 1999; Meyer and Peters, 2003].

The method is applicable for weakly bound ligands allowing quantification of the extent of binding strength in terms of association and dissociation constant in the mM-µM range [Meyer and Peters, 2003]. It is one of the popular techniques in pharmaceutical industries for routine drug screening and discovery due to its (a) ease of implementation and (b) both qualitative and quantitative robustness to answer fundamental, applied biological and biomedical questions related to molecular interactions between ligands and targets [Wagstaff, et al., 2013].

In the STD_{on} spectrum, the effect of saturation can propagate along the entire macromolecular length via an extremely effective intramolecular spin-diffusion process. This is simply because of the presence of a large network of protons strongly coupled to each other due to dipole-dipole interactions. [Angulo, et al., 2010; Angulo and Nieto, 2011; Cala and Krimm, 2015; Krishnan, 2005]. The saturation of protein proton signal gets progressively transferred to the binding ligands associated to the macromolecules through intermolecular dipolar interaction. On the other hand, the ligands that do not bind with the target will not receive any saturation. The experimental set up requires some specific conditions to be maintained. For example, to obtain an effective STD NMR spectrum, samples containing target: ligand concentration in the range of 1: 10 to 1: 100 are advisable to be used. Generally, in the case of protein or HA, chemical shift regions either of aliphatic resonances (–1 to 3 ppm) or aromatic resonances (6-8 ppm) are saturated in the case of ^1H–^1H STD_{on} NMR, ensuring this region contains target resonances only. The STD_{off} spectrum is recorded with the saturation pulse applied beyond 20 ppm in the case of ^1H–^1H STD NMR to avoid the transfer of any undesired polarization to the target and ligand resonances. The desired STD difference spectrum (STD_{Diff}) is obtained by subtracting the STD_{on} from the STD_{off}. Here, the ligands that are spatially proximal to the target will receive the saturation transfer exhibiting the signals in the STD_{Diff} spectrum. Resonances observed in the STD_{Diff} spectrum for the various part of the ligand are, in general, appear with varying intensities indicating the variable amount of saturation transfer received by the different ligand nuclei based on their spatial distance from the target. The component of the ligand closest to the target will receive the maximum saturation, and those farthest from the target receive the least. Hence, Group Epitope Mapping (GEM) is a prominent advantage of this method [Mayer and Meyer, 2001]. It enables identifying the parts of binding ligands that are in close contact with the target [Monaco, et al., 2017].

The saturation transferred to each part of the ligand from the target can be calculated by integrating the resonances that appeared in STD_{diff} relative to the same resonances in STD_{off} as depicted in equation 2.22. The part of the ligand with the highest relative STD signal is assumed to receive 100% saturation, while for all other resonances, the saturation is calculated relative to the 100% one.

$$I_{STD} = \frac{I_0 - I_{sat}}{I_0} \text{.....(2.22)}$$

Here, I_o : resonance intensity appeared in STD_{off}, and I_{sat} : resonance intensity appeared in the STD_{diff} spectrum. I_{STD} : line integral parameter that allows the quantification of saturation transfer from target to the ligand.

To achieve optimum saturation, the parameter 'saturation time (t_{sat})' needs to be optimized while acquiring the STD spectrum. For this, the STD spectrum is acquired at different saturation time, and the maximum saturation obtained at a particular time is taken as t_{sat} for further experiments [Muñoz-García, et al., 2018; Tanoli, et al., 2015; Vasile et al., 2018]. The binding strength of the ligand-protein complex in terms of the dissociation constant (K_D) can also be determined from STD experiments measured for a series of sample with variable ligand: protein ratio. The intensities appeared for these set of samples in STD_{diff} spectrum are plotted as a function of ligand or protein concentration and further fitted using hyperbolic functions similar as Michaelis Menten equation [Fisher, 2014; Longstaffe and Simpson, 2011; Ludwig and Guenther, 2009; Viegas et al., 2011]. In the following, the STD pulse sequence employed in the present Thesis has been discussed.

(i) Heteronuclear STD ($^{19}F–^{1}H$)

STD NMR methods have been evolved over the years, and many of these pulse sequences are discussed in the review by Wagstaf et al., 2013 [Wagstaff et al., 2013]. Heteronuclear multidimensional STD and ^{19}F STD methods are becoming more amenable due to the latest NMR technologies. In ^{19}F observe forward STD ($^{19}F–^{1}H$) experiments (similar to standard $^{1}H–^{1}H$ STD), ^{1}H peaks of the target are saturated while the transfer of this saturation to the ^{19}F moiety of ligand (organofluorines) is monitored. ^{19}F offers a method to observe specific nuclear interactions to differentiate chemical positions that are hard to distinguish in ^{1}H NMR spectra. ''Reverse'' $^{19}F–^{1}H$ STD saturates ^{19}F peaks of ligand and observes transfer to ^{1}H (of target) to provide validation of specific contact points. The requirements for carrying out these experiments are (a) fluorinated samples and (b) NMR hardware simultaneously exciting and decoupling ^{1}H and ^{19}F ideally.

The pulse sequences for acquiring $^{1}H–^{1}H$ STD (solvent suppressed) and $^{19}F–^{1}H$ STD NMR have been shown in figure 2.14 (a & b), respectively. In the present Thesis, Bruker standard pulse sequence using a selective Gaussian pulse for saturation of target resonances is used for acquisition of $^{1}H–^{1}H$ STD NMR, and this pulse sequence is modified for carrying out fluorine observed $^{1}H–^{19}F$ STD NMR [Longstaffe, et al., 2010; Ribeiro et al., 2015]. The use of a shaped pulse offers the following advantages (a) uniform excitation of the selected region and (b) reduces side-band artifacts (c) to achieve the desired selectivity.

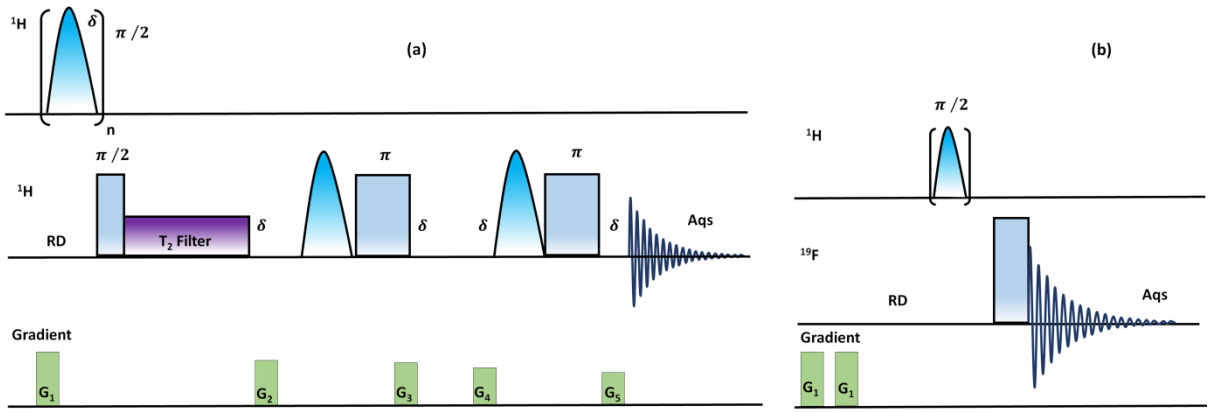

Figure 2.14: Basic pulse sequence for recording (a) ^{1}H–^{1}H and (b) ^{19}F–^{1}H STD NMR. Blue bars represent the RF pulses and green bars are gradient pulses; Guassian shaped pulse: selective pulse; RD: relaxation delay; Aqs: acquisition time.

2.6.2 OVERHAUSER DYNAMIC NUCLEAR POLARIZATION (ODNP):

Dynamic nuclear polarization (DNP) is one of the hyperpolarization techniques well known for sensitivity enhancement in NMR [Slichter, 2014]. The basic principle of DNP involves transfer of the large electron polarization of an endogenous or exogeneous paramagnetic polarizing agent to the neighbouring nuclear spins of the sample of interest by perturbing the equilibrium electron population through microwave (MW) irradiation near or at the electron paramagnetic resonance transition. Paramagnetic probes like free radicals are added to the sample as a source of exogeneous electron spins. There are, in principle, four mechanisms known for the electron to nucleus spin polarization transfer, *i.e.,* (a) cross relaxation between the electron and nuclear spin due to the Overhauser effect [Dwek, et al., 1969; Müller-warmuth and Meise-Gresch, 1983] (b) cross effect [Hwang and Hill, 1967] (c) solid effect [Smith, et al., 2012] and (d) thermal mixing [Wind and Duijvestijn, 1985].

In the current Thesis, DNP in the liquid state known as Overhauser DNP has been explored that relies on the first (a) mechanism. ODNP is the earliest known hyperpolarization technique in NMR based on the nuclear Overhauser enhancement principle that has been theoretically proposed sixty-five years ago [Armstrong and Han, 2009; Carver and Slichter, 1953; Hausser and Stehlik, 1968; Hubbard, 1966; Overhauser, 1953]. ODNP is generated during continuously saturating the electronic transitions of free radicals by microwave EPR, followed by acquiring the NMR spectra of the nuclei present in the liquid state at room temperature [Abragam, 1953; Bates, 1993]. EPR saturation enables the cross-relaxation between electron and nucleus, leading to the change of population distribution at thermal equilibrium (Boltzmann population). The resultant population distribution results in an enhanced NMR signal. Figure 2.15 represents pictorial explanation of the principle of ODNP mechanism for two-spin- ½ model systems (electron spin and nuclear spin) and the relevant relaxation processes involved [Chandrakumar, 2010]. The population distribution at thermal equilibrium for energy levels of two spin half system (electrons and nuclei) has been given in figure 2.15 (a). W_0, W_1, and W_2 represent the relaxation probability of zero, single and double quantum transitions, respectively. Here, the difference in the population of NMR energy level is given as (P_1–P_2= 2δ = P_3–P_4). The saturation of both the electron spin (EPR) transitions (1 to 3 and 2 to 4) by continuous MW irradiation changes the relative population of the respective energy levels as P_1=P_3; P_2=P_4 and is depicted in figure 2.15 (b). If W_0 is considered as the only operating mechanism for relaxation between energy levels 1 and 4, the relative population distribution of each energy level that appears after equilibrating the population of energy levels 1 and 4 is represented in figure 2.15 (c). The population difference amongst the perturbed NMR energy levels (figure 2.15 (c)) is

given as $P_1-P_2 = 2(\Delta+\delta) = P_3-P_4$. This 2Δ excess gain in population compared to the thermal equilibrium case has been achieved as a result of the hyperpolarization phenomenon [Bates, 1993; Chandrakumar, 2010; Dey, 2019; Potenza, 1972].

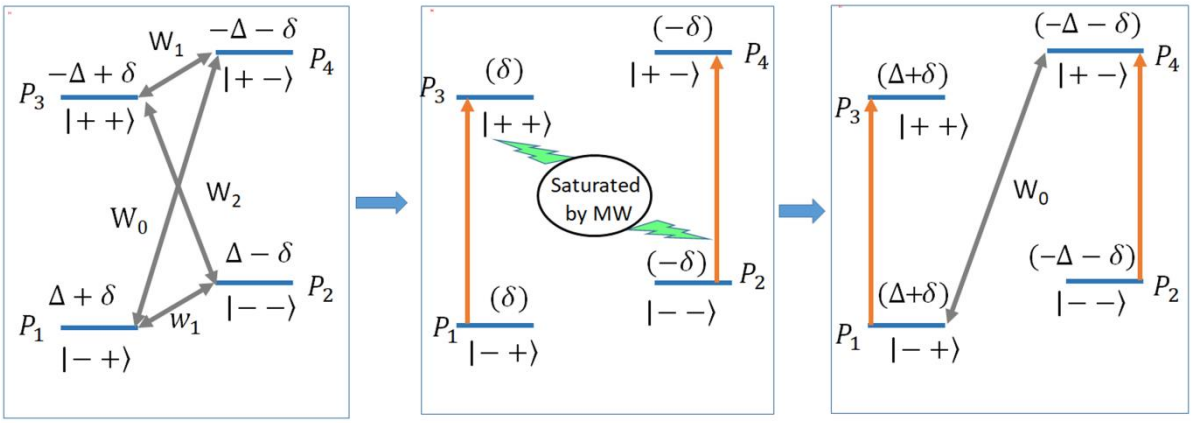

Figure 2.15: Underlying principle of ODNP mechanism: (a) energy levels of electron-nuclear two-spin-1/2 systems at thermal equilibrium along with all the relaxation transition probabilities. Here each state is labeled as $|m_e m_n\rangle$; $\gamma_n > 0$, $\gamma_e < 0$. $\pm\Delta$ are relative populations of electron spin energy levels and $\pm\delta$ are relative populations of nuclear spin energy levels at equilibrium. W_i' s indicate the probability of zero, single and double quantum relaxation transitions as indicated by the subscripts. (b) The population of energy levels after simultaneously saturating both the electron spin transitions by microwave (MW) ($P_1=P_3$; $P_2=P_4$). (c) The population of energy levels when zero quantum transition is the sole relaxation mechanism operating, equilibrating the relative populations of the levels 1 and 4.

The relative NMR signal enhancement (A) achieved due to excess in population when W_0 operates is written as:

$$A = \left(\frac{I_z - I_0}{I_z}\right) = \left(\frac{\Delta}{\delta}\right) = -\left(\frac{\gamma_e}{\gamma_n}\right) \text{.....(2.23)}$$

On the other hand, when W_2 is the operating mechanism, the enhancement is written as:

$$A = \left(\frac{I_z - I_0}{I_z}\right) = -\left(\frac{\Delta}{\delta}\right) = \left(\frac{\gamma_e}{\gamma_n}\right) \text{.....(2.24)}$$

γ_e, γ_n are the magnetogyric ratios of electron and nuclear spin respectively.

The overall relative ODNP enhancement of NMR signal may be deduced as equation 2.25 in terms of all the relaxation transition probabilities (W_0, W_1, and W_2). W_b is relaxation transition probability in the absence of the radical.

$$A = \left(\frac{W_2 - W_0}{W_2 + 2W_1 + W_0 + W_b}\right)\left(\frac{\gamma_e}{\gamma_n}\right) \text{.....(2.25)}$$

The following section gives a brief overview of the experimentally measured ODNP parameters explored in the current Thesis [Banerjee, et al., 2016, 2019; Dey, et al., 2017; George and Chandrakumar, 2014]..

(i) Parameters of ODNP:

Figure 2.16 represents the primary pulse sequence for ODNP used in the current study. This pulse sequence is employed to measure the ODNP enhancement factor.

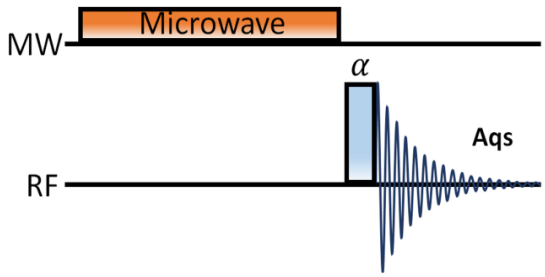

Figure 2.16: Basic pulse sequence for ODNP experiment. MW: electronic channel; Microwave: MW saturation pulse; RF: radiofrequency channel for nuclei; α: hard pulse applied on nuclei; Aqs: acquisition.

The enhancement factor A under steady-state ODNP conditions (enhancement remains unchanged with increasing MW irradiation time) can be expressed in terms of experimentally observable parameters, *i.e.,* the EPR saturation parameter (s) of the added free radical, the substrate nuclear spin relaxation leakage factor (f) and the ODNP coupling parameter (ξ) as presented in equation 2.26:

$$A = \xi f s \frac{\gamma_e}{\gamma_n} \text{.....(2.26)}$$

The saturation parameter s determines the saturation efficiency of the radical EPR lines by MW irradiation and is given as:

$$s = \left(\frac{S_z - S_0}{S_z} \right) \text{.....(2.27)}$$

s can be determined using the following procedure: ODNP enhancement A is measured and plotted as a function of microwave power P. The resulting straight-line plot between A and P is extrapolated to infinite power (P_∞) to get the 'ultimate' enhancement A_∞ (s =1 for A_∞). The experimental value of s can be inferred from this value and the observed maximum enhancement employing equation 2.28:

$$s = \left[\frac{A}{A_\infty} \right] \text{.....(2.28)}$$

Further, the leakage factor (f) is defined as the ratio of the auto-relaxation rate of the nuclear spin (ρ^I) to its net relaxation rate ($\rho_I = \rho^I + \rho^o$) where ρ^o is defined as the relaxation rate due to relaxation mechanisms other than the fluctuating electron-nuclear interactions. Hence, f consists of the effect of all relaxation mechanisms except the electron-nuclear relaxation mechanism. Experimentally, it is determined by measuring T_1 of the substrate nuclear spins with and without added free radical.

$$f = \left(1 - \frac{T_1}{T_{1,0}} \right) \text{.....(2.29)}$$

where T_1 is the longitudinal relaxation time of the substrate nuclear spins in the presence of radical, while $T_{1,0}$ is the corresponding quantity in the absence of the radical.

ξ known as the coupling parameter characterizes the fluctuating interaction between the electron and nuclear spins under ODNP conditions. It can also be defined as the ratio of the electron-nuclear cross-relaxation rate (σ^{IS}) and the nuclear auto relaxation rate (ρ^I) given in equation 2.30.

$$\xi = \frac{W_2 - W_0}{W_2 + 2W_1 + W_0} = \frac{\sigma^{IS}}{\rho^I} \text{.....(2.30)}$$

Here W_0, W_1, and W_2 are the rates of the zero quantum, single quantum and, double quantum relaxation transitions, respectively.

This interaction, which in general could be dipolar or scalar in origin, or of mixed nature, is characterized by the electron-nuclear correlation time reflecting the motional dynamics in the solution-state. Hence, the coupling parameter can be considered as an experimentally derived parameter that can account for molecular motions in solution. One may exploit this idea to probe molecular interactions between a ligand-target pair by monitoring the changes in the ligand's coupling parameter in the absence and presence of the target where the target is labelled with a paramagnetic agent that serves as the electron polarization source. ODNP experiments therefore offer a unique window for probing molecular dynamics on the timescales of the order of 10-1000 picoseconds with improved sensitivity owing to the free radical-solute interaction besides focussing only on the sensitivity enhancements as a dominant application. Discussions on the prevailing applications of ODNP are addressed in various recent literature [Bennati, et al., 2010; Cheng, et al., 2012; Dey and Banerjee, 2019; Franck, et al., 2013a; Kaminker, et al., 2015; Lingwood, et al., 2010a, 2010b; Pylaeva, et al., 2017].

The variation of coupling parameter values as a function of varying field and correlation time based on different types of electron-nuclear interactions is discussed in the literature in terms of spectral density functions. Hubbard is probably the first researcher who proposed to model these electron-nuclear spin interactions by characterizing the spectral density function in the context of ODNP [Hubbard, 1966]. Relaxation mechanisms due to translational motion mediated and rotational motion mediated dipolar interaction between electron-nuclear spins have been modelled in the literature and have been discussed in great detail. However, such a discussion is beyond the scope of the present Thesis. Thorough analysis of the rotation and translation mediated dipolar models enables the understanding and extraction of dynamical information of molecules in the solution-state from ODNP measurements of different molecular systems at a fixed field, as shown in figure 2.17. The plot presented in figure 2.17 demonstrates the variation of the coupling parameter as a function of motional correlation time at a fixed EPR frequency (ω_s) of 9.6 GHz according to different Hubbard's model [Dey, 2019].

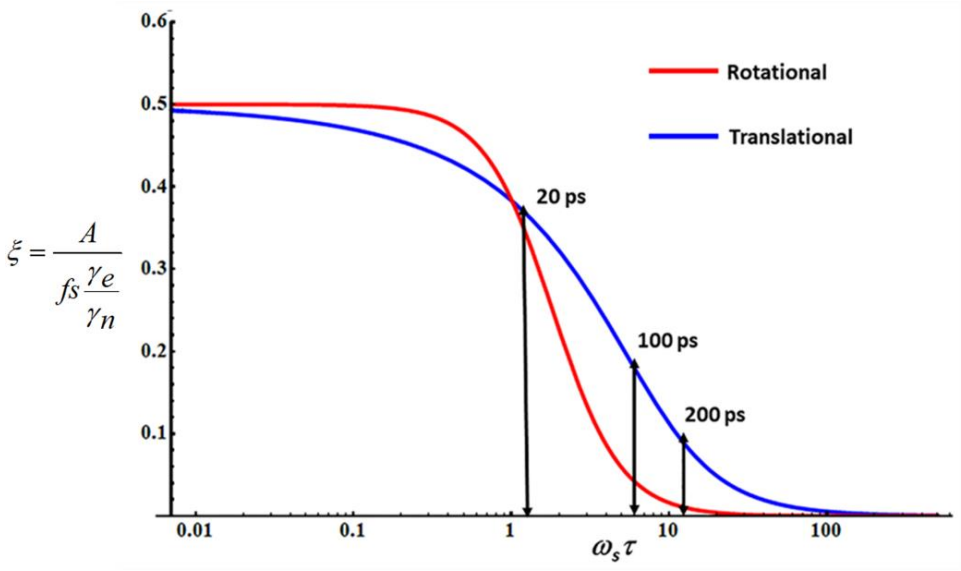

Figure 2.17: Plot between coupling parameter (ξ) *and* $\omega_s \tau$ for electron-nuclear (^{1}H) dipolar interaction mediated by translational and rotational motion at 9.6 GHz. The coupling parameter values for the different correlation time shown in the figure can be obtained from the intersection of the arrow with the y-axis.

It is known that electron-nuclear interaction can be scalar (direct) or dipolar (through space) in nature. The resultant magnitude and sign of steady-state enhancement in ODNP depend on the type of interactions or the compensation of these interactions by each other. In ^{1}H ODNP experiments, a negative enhancement appears because the interaction between the electron and nuclear spin is purely dipolar, while ^{19}F ODNP measurements exhibit a resultant of mixed dipolar and scalar electron-nuclear interaction. The ^{19}F mixed ODNP is not separable based on measurements at a single field and at a fixed temperature. Therefore, the extraction of the motional correlation time from the ^{19}F coupling parameter is not straightforward [Borah and Bates, 1981b]. But, the coupling parameter extracted from the resultant ^{19}F ODNP enhancement can be interpreted as a probe of the molecular motions as well as the chemical environment of interacting electron spins (radical) and the nuclear spin (substrate).

….